Adsorption Performance Indicator for Power Plant CO_2 Capture on Graphene Oxide/TiO_2 Nanocomposite

Nazari Kudahi, Saeed; Noorpoor, Ali Reza*[+]

School of Environment, College of Engineering, University of Tehran, P.O. Box 14155-6135 Tehran, I.R. IRAN

Mahmoodi, Niyaz Mohammad

Department of Environmental Research, Institute for Color Science and Technology, Tehran, I.R. IRAN

ABSTRACT: *This study presents the adsorption performance indicator for the evaluation of thermal power plant CO_2 capture on mesoporous graphene oxide/TiO_2 nanocomposite. To begin, this adsorbent was synthesized and characterized using N_2 adsorption-desorption measurements (BET and BJH methods), X-Ray Diffraction (XRD), Field Emission Scanning Electron Microscopy (FE-SEM) and FT-IR spectroscopy. Subsequently, the pure single-component adsorption isotherms measured at 298 K and the Ideal Adsorbed Solution Theory (IAST) solved with direct search minimisation were applied to estimate the selectivity of the synthesized mesoporous graphene oxide/TiO_2 nanocomposite for CO_2 over N_2 and predict CO_2 adsorption capacity in the CO_2:N_2 binary gas mixtures, including the molar ratio of 5:95, 10:90 and 15:85. Finally, the results validated by the breakthrough experiments at a fixed-bed column were applied to estimate the Adsorption Performance Indicator (API) for the evaluation of CO_2 separation from N_2 in the Pressure Swing Adsorption (PSA) process with respect to different types of thermal power plants.*

KEYWORDS *CO_2 capture; Thermal power plants; Adsorption performance indicator; Graphene oxide/TiO_2 nanocomposite; Ideal adsorbed solution theory; Breakthrough experiments.*

INTRODUCTION

The increase in the use of conventional fossil fuels such as coal, oil, and natural gas as a result of rapid economic growth has the serious damage on our environment and this trend has been led to increasing the emission of carbon dioxide as the main anthropogenic greenhouse gas [1]. The atmospheric carbon dioxide concentration has increased from 280 ppm before industrial revolution to 400 ppm in 2013 [1]. Without greenhouse gas mitigation policies, the atmospheric CO_2-equivalent concentration will reach to 600-1500 ppm [1]. According to scientific literature, there are different approaches to control greenhouse gas emissions. Improving energy efficiency, increasing the consumption of the low carbon fuels (including hydrogen and natural gas), utilizing renewable energy (such as wind, solar, hydropower and bio-energy), using geoengineering techniques and applying CO_2 Capture and Storage (CCS) technologies are the major approaches to mitigate global climate change [1]. Efficient CO_2 capture from the large point sources such as power plants, cement industries,

* *To whom correspondence should be addressed.*

+ *E-mail: noorpoor@ut.ac.ir*

1021-9986/2019/3/293-307 *15/$/6.05*

refineries, metal industries and other anthropogenic sources are some of the most important priorities to reduce the global warming effect [2]. In this regard, several technologies with various degrees of maturity have been developed for pre-combustion and post-combustion CO_2 capture processes. The main technologies include absorption, adsorption, membrane separation, chemical looping, hydrate-based separation and cryogenic distillation [1,2,3]). Absorption technology requires significant amounts of heat, which leads to the energy penalty for absorbent regeneration [4]. Furthermore, this technology has environmental impacts related to the sorbent degradation [1,2,3]). On the other hand, membrane gas separation technology is in the infancy stage and more studies are required to develop this technology [1,2,3]). The chemical looping process is under development and there is not any large plant operation experience. In addition, this technology has serious technical problems such as low fluxes and fouling [1]. Hydrate-based separation as a new technology that uses chilled water requires more research and development [1]. Cryogenic distillation as an energy intensive technology conducted at very low temperature and this technology is feasible for very high carbon dioxide concentrations (approximately above 90% v/v) [1]. Therefore, adsorption technology which needs fewer energy requirements and has several competitive advantages too, including lower capital cost, simplicity of operation and applicability in the wide range of temperature and pressure conditions has been introduced as an attractive technology to control CO_2 emissions [2,5]. Solid adsorbents which are the main important part of this technology allow the selective separation of CO_2 from the flue gas mixture as a result of different interaction forces between CO_2 molecules and the solid surface [6]. Recently, a group of solid adsorbents developed based on graphene and graphene oxide has been studied by scholars [2,6]. These adsorbents have some advantages as a result of the unique combination of graphene's chemical, mechanical, structural and thermal properties [2,6] such as high specific surface area and lowered production cost [2,6]. These properties make them more attractive in comparison with other conventional adsorbents including carbon fiber, metal organic frameworks, porous silica, porous polymers, zeolites, alumina, activated carbon and metal oxides [2]. The above mentioned features introduce graphene and graphene oxide-based adsorbents as the next generation of CO_2 adsorbents [2,6]. Therefore, great efforts have been made to explore CO_2 capture on these adsorbents since 2012 [6]. The determination of pure CO_2 uptake on several graphene/graphene oxide based adsorbents has been the main aim of these studies [2, 6-12]. Therefore, there is a literature gap to calculate CO_2 adsorption performance on these adsorbents in the mixed-gas system especially in the binary mixed-gas system which has different CO_2 partial pressures similar to CO_2 concentration in the flue gas of thermal power plants. Determination of CO_2 adsorption capacity in the multicomponent gas system on graphene and graphene oxide-based adsorbents has been recommended for future research on these adsorbents [2]. On the other hand, determination of CO_2 selectivity over other gases such as N_2 on different adsorbents to evaluate the performance of these adsorbents is one of the most important challenges for development of them [2,6]. CO_2 concentration is commonly in the range of 5%-15% depending on the fuel type fired in the combustion process, and the type of thermal power plants [13,14]. In this study, the selectivity of CO_2 over N_2 and CO_2 adsorption capacity in the binary mixed-gas system on the synthesized mesoporous graphene oxide/TiO_2 nanocomposite are theoretically and experimentally determined by the ideal adsorbed solution theory solved with direct search minimisation and the breakthrough experiments at a fixed bed column. The prediction of multi-component gas adsorption isotherms which is used to design the adsorption separation units has been studied by scholars with different models. One of the most famous models is the ideal adsorbed solution theory [15]. This model has the appropriate ability to anticipate multi-component adsorption isotherm data [15]. The applicability of the Ideal Adsorbed Solution Theory (IAST) to predict CO_2 selectivity over N_2 from the single component adsorption isotherm has been reported by some scholars [15-21]. Scholars apply this model to predict CO_2 adsorption uptake in the gaseous mixtures of CO_2/N_2 (or CO_2/CH_4) and determine selectivity of CO_2 over N_2 (or CH4) on MCM-41, MOF-14, different porous carbon adsorbents and biomass-based activated carbons ([16-21]. Recently, some scholars have proposed the new indicator entitled the adsorption performance indicator to compare the promising adsorbents such as metal-organic frameworks

and biomass-based activated carbons for separation CO_2 from CH_4 in the pressure swing adsorption process. This indicator merges three important parameters, including working capacity, selectivity and the heat of adsorption to screen the novel adsorbents for the gas separation [21,22]. For the first time in this study, the adsorption performance indicator is applied to compare the potential of the synthesized mesoporous graphene oxide/TiO_2 nanocomposite as the promising and energy-efficient carbon dioxide adsorbent [12] with other reported adsorbents for thermal power plant CO_2 capture.

In sum, the main objectives of this study are illustrated as follows:

-Determination of CO_2 adsorption capacity and CO_2 selectivity over N_2 on the synthesized mesoporous graphene oxide/TiO_2 nanocomposite in the binary mixed-gas system using the ideal adsorbed solution theory solved with direct search minimisation with respect to different CO_2 concentrations in the flue gas of thermal power plants.

-Validation of CO_2 adsorption capacity in the binary mixtures by the breakthrough experiments at a fixed bed column and estimation of the uncertainty of it using a combined uncertainty calculation method.

-Evaluation using the synthesized mesoporous graphene oxide/TiO_2 nanocomposite in comparison with other reported adsorbents for thermal power plant CO_2 capture by calculating the Adsorption Performance Indicator (API).

EXPERIMENTAL SECTION

Synthesis of mesoporous graphene oxide/TiO_2 nanocomposite

Graphene oxide was prepared from graphite powder (LOBA Chemie) based on the improved Hummer's procedure [12]. A one-step colloidal blending procedure was applied to prepare graphene oxide/TiO_2 nanocomposite (GO to TiO_2 mass ratio=0.1). According to this procedure, 0.2 g of graphene oxide was dispersed into the deionized water by ultrasonication for 0.5 h then 2 g of TiO_2 powder (Degussa) was added to the prepared graphene oxide suspension. After sonication of the final mixture for 1.5 h, graphene oxide/TiO_2 homogeneous mixture was prepared with a further stirring at room temperature for 12 h. After filtering and drying, mesoporous graphene oxide/TiO_2 nanocomposite was prepared at room temperature [12].

Characterization of graphene oxide/TiO_2 nanocomposite

The structure and surface morphology of the synthesized graphene oxide/TiO_2 nanocomposite were studied by field emission scanning electron microscopy (Hitachi S-4160, Japan), wide angle X-ray diffraction (PANalytical, Netherlands), N_2 adsorption-desorption measurements using BET and BJH methods (Microtrac Belsorp-mini II, Japan) and FT-IR spectra (400-4000 cm^{-1}) (Perkin-Elmer Spectrum One FT-IR Spectrometer, U.S.A).

Pure gas adsorption measurements

The measurement of pure CO_2 and pure N_2 adsorption equilibrium isotherms on the synthesized graphene oxide/TiO_2 nanocomposite were volumetrically carried out by Microtrac Belsorp- max adsorption apparatus (Japan). Adsorption isotherms were measured at 298 K and pressured up to 100 kPa. For desorption of any moisture and organic compounds, all of the samples were degassed under vacuum and at 393 K for 24 h. Ultra high purity grade CO_2 and N_2 gases (99.9%) were applied during the tests of this study.

Validation of CO_2 adsorption capacity in the binary mixed-gas system

Binary breakthrough adsorption tests of CO_2/N_2 system were conducted in a fixed-bed setup packed with the synthesized graphene oxide/TiO_2 nanocomposite (Fig. 1). LNI SONIMIX 2106 (programmable gas divider, Switzerland) was utilized to generate the simulated flue gas mixture, (including CO_2 and N_2) with CO_2 concentration of 5-15%. The multi-component gas analyzer (MRU DELTA 1600 S-IV, Germany) equipped with a CO_2 Non-Dispersive InfraRed (NDIR) detector was applied to analyze the CO_2 concentration at the outlet of the experimental setup. Before each experiment, for desorbing any moisture and organic compounds, the samples of the synthesized graphene oxide/TiO_2 nanocomposite (approximately 0.7 g) were degassed at 393 K under vacuum for 24 h. The simulated flue gas, including CO_2:N_2 mixtures of 5:95, 10:90 and 15:85 were fed to the adsorption fixed-bed column (glass, 10 cm in height and 1 cm in diameter) and CO_2 adsorption The dynamic CO_2 adsorption capacity (q) calculated as a function of the feed gas CO_2 concentration is illustrated as in the following [23-25]:

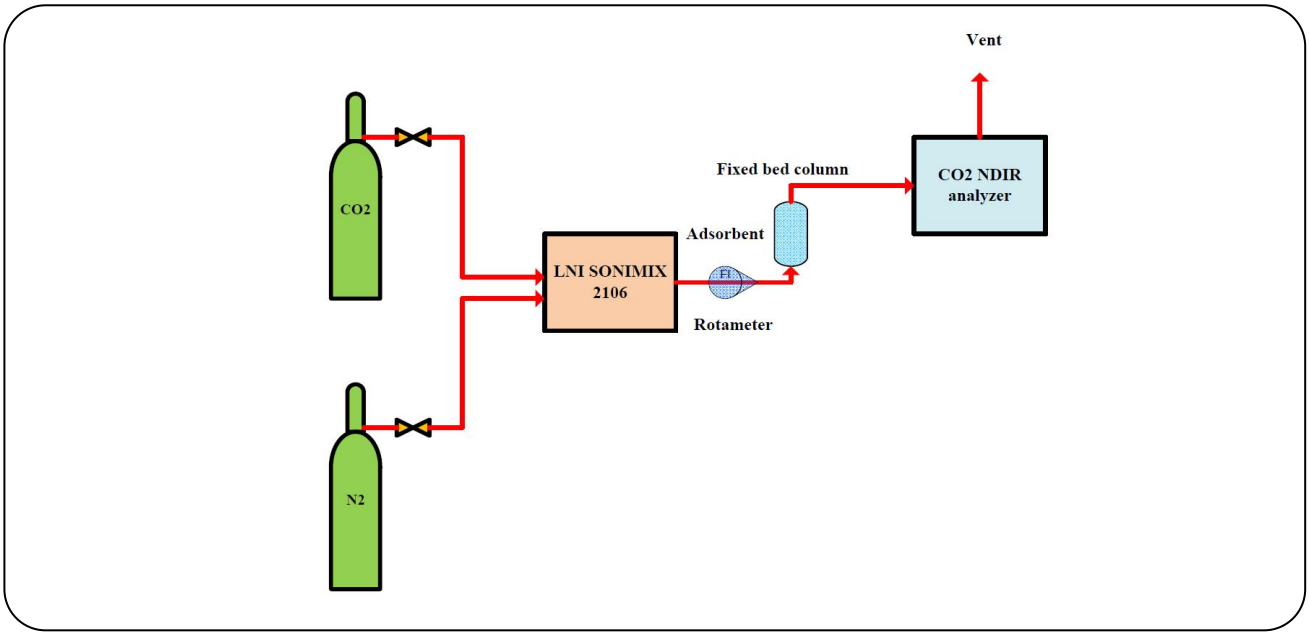

Fig. 1: Experimental setup for determination of CO_2 capture on graphene oxide/TiO_2 nanocomposite.

$$q = \frac{Q_F c_0 t_q}{m_s} \quad (1)$$

Where Q_F is the volumetric flow rate of the feed gas, c_0 is the inlet CO_2 concentration, m_s is the mass of adsorbent loaded in the bed and t_q is the stoichiometric time, which is calculated from the breakthrough profile as follows:

$$t_q = \frac{C_{CO_2,in} t_s - \int_{t_b}^{t_s} C_{CO_2}(t)\,dt}{C_{CO_2,in}} \quad (2)$$

Where, t_s, t_b, and $C_{CO2}(t)$ are saturation time (sec), breakthrough time (sec) and CO_2 concentration at time t, respectively. Saturation and breakthrough times are defined as the times when outlet CO_2 concentration reaches to 5% and 95% of inlet CO_2 concentration respectively [23]. The relative error (*RE*) applied in this study to analyze the error between the experimental CO_2 adsorption capacity and the calculated CO_2 adsorption capacity is illustrated, below: [21].

$$RE(\%) = \left|\frac{q_{meas} - q_{calc}}{q_{meas}}\right| \times 100 \quad (3)$$

Where q_{meas} is the experimental CO_2 adsorption capacity and q_{calc} is the calculated CO_2 adsorption capacity predicted by the Ideal Adsorbed Solution Theory (IAST) solved with the direct search minimisation**.** Using the combined uncertainty calculation method, the uncertainty of CO_2 adsorption capacity is determined. According to this method, the absolute combined standard uncertainty of CO_2 adsorption capacity is illustrated as follows [26]:

$$u_c(q) = q \times \sqrt{\left(\frac{u(Q_F)}{Q_F}\right)^2 \times \left(\frac{u(c_0)}{c_0}\right)^2 \times \left(\frac{u(t_q)}{t_q}\right)^2 \times \left(\frac{u(m_s)}{m_s}\right)^2} \quad (4)$$

Where, $u_c(q)$ is the combined standard uncertainty of CO_2 adsorption and $u(Q_F/Q_F)$, $u(c_0/c_0)$ and $u(m_s)/m_s$ and $u(t_q/t_q)$ are the relative uncertainty of the volumetric flow rate of the feed gas, the inlet CO_2 concentration, the mass of adsorbent loaded in the column and the stoichiometric time respectively.

THEORETICAL SECTION

Estimation of CO_2 selectivity over N_2 and prediction of CO_2 adsorption capacity using the ideal adsorbed solution theory solved with the direct search minimisation

The ideal adsorbed solution theory assumes that the adsorbed phase and the ideal gas phase are in equilibrium

and the adsorbed phase as an ideal phase follows equations should be solved to predict multicomponent gas adsorption on different adsorbents [27]:

$$P_{tot} y_i = P_i^0 x_i \qquad i = 1,2,3...N \tag{5}$$

$$\sum_{i}^{N} x_i = 1 \tag{6}$$

$$n_i = f_i\left(P_i^0, T\right) \qquad i = 1,2,3...N \tag{7}$$

$$\frac{\pi_i A}{RT} = \int_0^{P_i^0} n_i d\left(\ln\left(P_i^0\right)\right) \qquad i = 1,2,3...N \tag{8}$$

Where P_{tot} (kPa) and y_i are the total pressure of gaseous mixture on the adsorbent surface and the molar fraction of component i of the non-adsorbed mixture respectively. The molar fraction of component i in the adsorbed phase, the total number of components and the adsorption amount of component i from the adsorption isotherm are defined by x_i, N and n_i (mol/kg), respectively. The surface pressure of component i, the equilibrium temperature, the specific spreading pressure of component i and the specific surface area covered by the adsorbed mixture are illustrated by the parameters, P_i^0 (kPa), T (K), π_i (kPa m) and A (m^2/kg), respectively [27]. When the spreading pressure ($\pi_i A/RT$) of each component has the same value, the system achieves equilibrium.

Therefore, the equilibrium condition is shown as in the following equation [27]:

$$\frac{\pi_i A}{RT} = constant \qquad i = 1,2,3...N \tag{9}$$

If the parameters, P_{tot}, y_i, and the single component adsorption equilibrium data are given, the problem can be solved. The substitution of variables causes the IAST equations to be reduced to a smaller system of iso-spreading pressure conditions. The spreading pressure is illustrated as the terms of molar fraction x_i by using an initial change of variable from P_i^0 to x_i replacing the Eq. (5)-(8). Spreading pressure acquired by this variable change is illustrated as [27]:

$$d\ln\left(\frac{P_{tot} y_i}{x_i}\right) = -\frac{1}{x_i} dx_i \tag{10}$$

Raoult's law [27]. The following algebraic-integral

The following equation represents the analytically integrated form of the spreading pressure for the Toth adsorption isotherm [27]:

$$\frac{\pi_i A}{RT} = \frac{y_i P_{tot} K_{Ti} q_{s,i}}{x_,} \tag{11}$$
$$F_1\left(\frac{1}{t_i}; \frac{1}{t_i}; \left(1+\frac{1}{t_i}\right); -\left(\frac{y_i P_{tot} K_{ti} q_{s,i}}{x_i}\right)\right)$$

Where ${}_2F_1$ illustrates the Gauss hypergeometric function. Using this spreading pressure, the iso-spreading pressure condition is set as a minimisation problem. Eq. (6) is used to calculate the objective function of the minimisation problem for the binary system. Therefore, the following function is obtained as [27]:

$$f_{binary}\left(x_1\right) = \left|\frac{\pi_1\left(x_1\right)A}{RT} - \frac{\pi_2\left(x_2\right)A}{RT}\right| \tag{12}$$

The selectivity for CO_2 over N_2 is estimated by the following equation [12]:

$$Selectivity = \left(\frac{x_{CO_2}}{x_{N_2}} \Big/ \frac{y_{CO_2}}{y_{N_2}}\right) \tag{13}$$

Where, x_{CO2} and x_{N2} are the mole fraction of components CO_2 and N_2 adsorbed on the adsorbent and y_{CO2} and y_{N2} show the mole fraction components of CO_2 and N_2 component in the gaseous mixture, respectively.

In this study, the fitting parameters related to the Toth model have been obtained by Levenberg- Marquardt algorithms using LAB Fit curve fitting software (V 7.2.48).

Determination of the adsorption performance indicator

Comparing different adsorbents with various natures for a specific separation process has the most important implication on developing them. For the gas separation by the adsorption process, the high uptake capacity and selectivity, as well as the low isosteric heat of adsorption, are the most important factors to evaluate an adsorbent. On the other hand, the results reported by some scholars show that these parameters solely are not appropriate to screen the adsorbents for the gas mixture separation [21,22]. Therefore, it is essential to introduce an indicator that combines these parameters for primary selection of the

adsorbents. To this end, the Adsorption Performance Indicator (API) for the bulk removal and the gas purification processes based on the balances among the three aforementioned parameters have been developed by the scholars as in the following [21,22]:

$$API = \frac{\left(S_{1/2} - 1\right)^{A} \times WC_1^{B}}{\left|Q_{ST,1}\right|^{C}} \quad (14)$$

Where, $S_{1/2}$, WC_1 and $Q_{st,1}$ are the selectivity of component 1 over component 2, the working capacity of component 1 and the isosteric heat of adsorption of component 1, respectively. In this study, the adsorption performance indicator is applied to compare the potential adsorbents for separating CO_2 molecules from N_2 molecules. In this regard, the exponent of working capacity (B) which has considerable importance has been established to 2 and the rest of exponents (A and C) have been considered to 1 [21]

RESULTS AND DISCUSSION

Mesoporous graphene oxide/TiO_2 nanocomposite characterization

Fourier Transform InfraRed (FT-IR) spectroscopy

The FT-IR spectra of graphene oxide, TiO_2 and graphene oxide/TiO_2 nanocomposite are illustrated in Fig. 2. The broad peak at 3398.09 cm^{-1}, 3337.22 cm^{-1} and 3345 cm^{-1} indicate the presence of surface O-H stretching vibrations (Figs. 2a, 2b and 2c) [28,29]. The C-OH stretching vibration peak at 3345 cm^{-1} in graphene oxide (Fig. 2c) has shifted to the higher wavenumber in graphene oxide/TiO_2 nanocomposite (3398.09 cm^{-1}) as a result of the Ti-O-C bond formation (Fig. 2a) [28,29]. The peaks at 1427.76 cm^{-1} and 1261.44 cm^{-1} are attributed to tertiary C-OH and epoxy C-O groups, respectively (Fig. 2a). The absorption peak at around 1626.78 cm^{-1} is related to the skeletal vibration of the graphene oxide sheets (Fig. 2a) [28,29]. For graphene oxide/TiO_2 nanocomposite, the C-O stretching vibration peak at 1040 cm^{-1} and the C=O stretching vibration of –COOH group peak at 1721cm^{-1} of graphene oxide have been completely disappeared (Figs. 2a and 2c) [28,29]. The strong absorption band at 672.26 cm^{-1} (in the synthesis of graphene oxide/TiO_2 nanocomposite) is probably related to the vibration modes of Ti-O-Ti and Ti-O-C bonds (Fig. 2a) [28,29]. This vibration mode is similar to the FT-IR spectrum of pure TiO_2 (Fig. 2b). These vibration modes

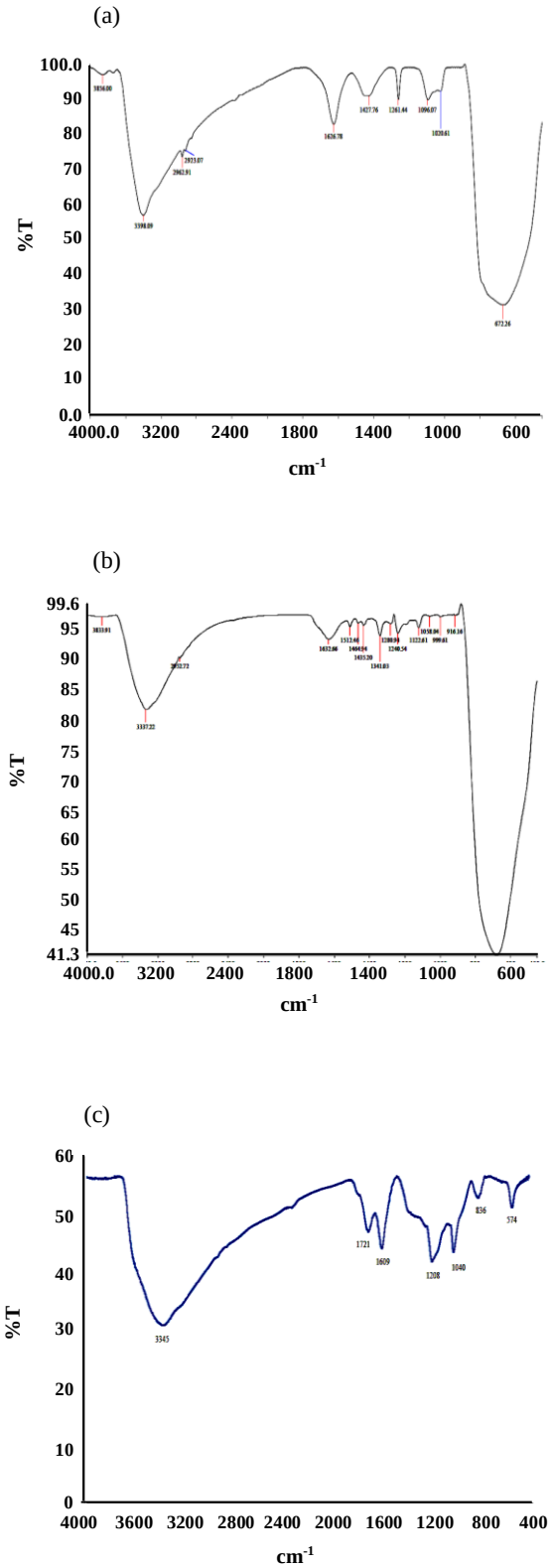

Fig. 2: FT-IR spectra of graphene oxide/TiO_2 nanocomposite (a), TiO_2 nanoparticles (b) and graphene oxide (c).

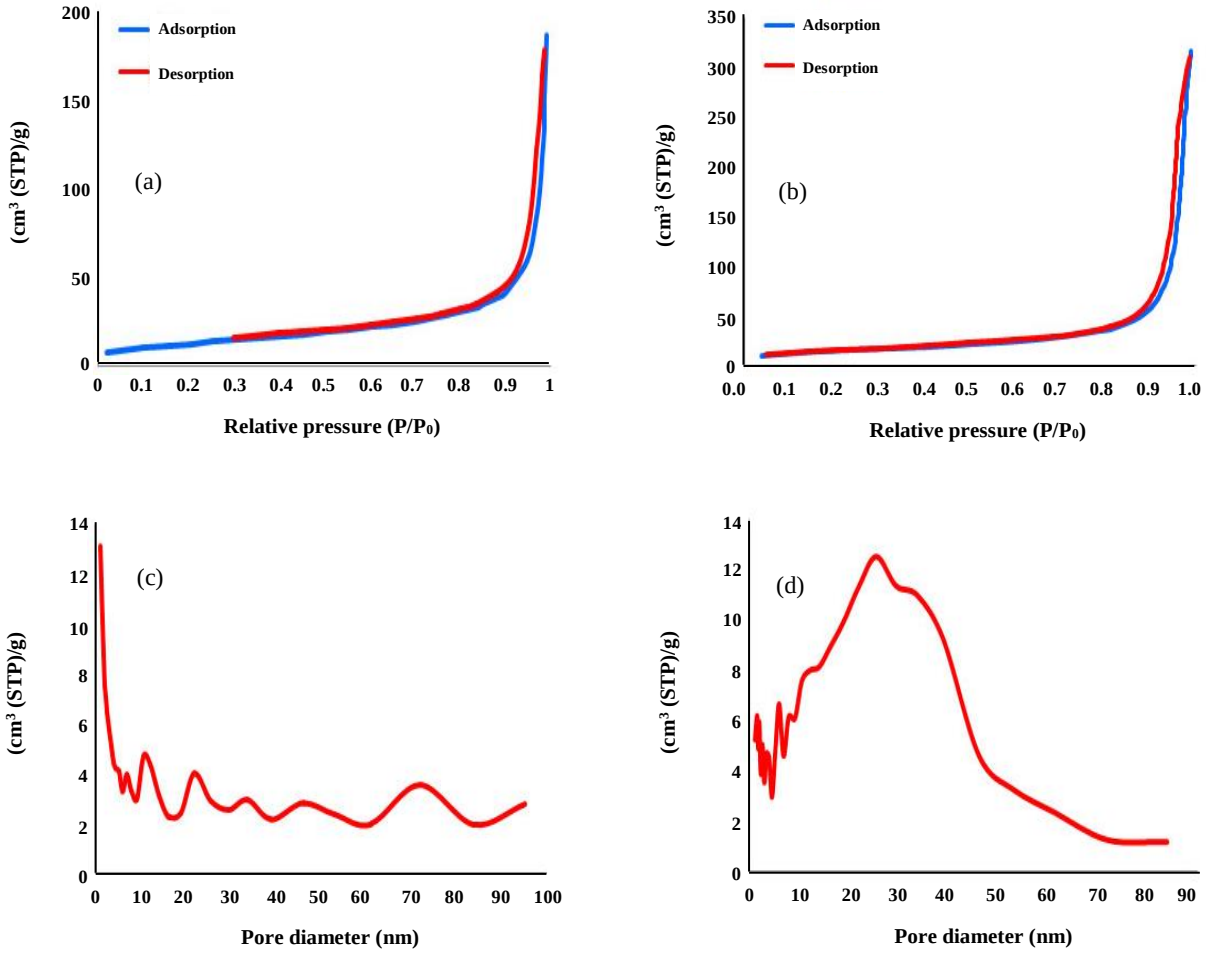

Fig. 3: N_2 adsorption-desorption isotherms at 77 K for TiO_2 nanoparticles (a), graphene oxide/TiO_2 nanocomposite (b), pore size distribution using BJH method for TiO_2 nanoparticles (c) and graphene oxide/TiO_2 nanocomposite (d).

indicate that the TiO_2 nanoparticles strongly bond to the graphene oxide sheets [28, 29].

Nitrogen adsorption–desorption isotherms

The identification of pore and textural structures of an adsorbent has the most significant implication on designing the related adsorption process [30]. This identification is performed by the adsorption/desorption measurements of Nitrogen at 77 K and subsequently using BET and BJH methods to calculate specific surface area and pore size distribution on the synthesized graphene oxide/TiO_2 nanocomposite and its major component (TiO_2 nanoparticles). Fig.3a and 3b shows a Type IV isotherm which is typical of the mesoporous compounds [31]. The specific surface area and total pore volume of the synthesized graphene oxide/TiO_2 nanocomposite as a result of incorporation TiO_2 nanoparticles between 2 D graphene oxide sheets in comparison with TiO_2 powder have been increased from 47.420 m^2/g to 96.367 m^2/g and 0.2864 cm^3/g to 0.4834 cm^3/g, respectively [6]. Furthermore, the average pore diameter has been increased from 24.319 nm to 37.051 nm. Fig.3 (c and d) obtained by applying BJH method shows that the pore size distribution in graphene oxide/TiO_2 nanocomposite is principally in the mesoporous range (6.946 nm to 46.13 nm). Moreover, the average pore size of this composite which has been estimated as 37.051 nm verified the mesoporous textural structure of it. The synthesized graphene oxide/TiO_2 nanocomposite does not show any limiting adsorption

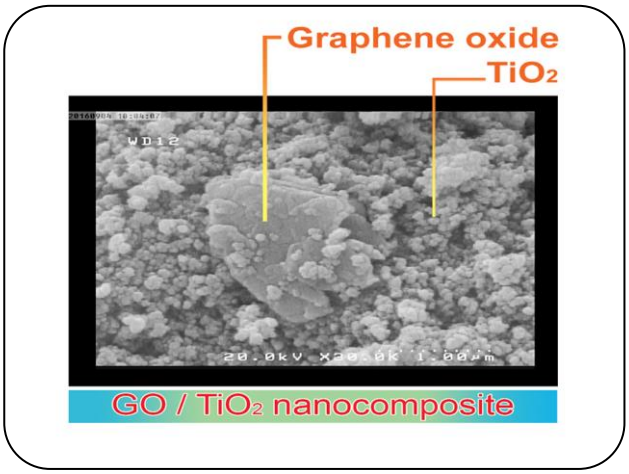

Fig. 4: FE-SEM image of graphene oxide/TiO_2 nanocomposite.

at high P/P_0 in adsorption/desorption isotherm. Therefore, it indicates that typical of a Type H3 hysteresis loop has been involved with the presence of non-rigid aggregates of plate-like particles forming slit-shaped pores [12,31]. This case is relevant to the presence of the graphene oxide nanosheets coated with TiO_2 nanoparticles and observed in the FE-SEM images (Fig. 4).

Field Emission Scanning Electron Microscopy (FE-SEM)

The microstructure of the synthesized mesoporous graphene oxide/TiO_2 nanocomposite has been characterized by FE-SEM image (Fig. 4). It has been clearly observed that the TiO_2 nanoparticles have been distributed on both sides of the graphene oxide nanosheets. The reciprocal electrostatic interaction between positively charged Ti^{4+} of TiO_2 and negatively charged oxygen atoms of graphene oxide has been led to the heterostructure of mesoporous graphene oxide/TiO_2 nanocomposite [32].

X-ray diffraction pattern (XRD)

The XRD patterns, the synthesized graphene oxide, pure graphite as its precursor and the synthesis mesoporous graphene oxide/TiO_2 nanocomposite are illustrated in Figs. 5 a and 5b, respectively. The XRD pattern of graphene oxide and graphite show the characteristic peak from (002) diffraction at $2\theta=10.77^o$ correlated to a d-spacing of 8.1 Å and a major peak from (002) at $2\theta=26.52^o$ correlated to a d-spacing of 3.3 Å, respectively (Fig. 5a). The intercalation of oxygen functional groups and water molecules during Hummer's process might lead to the large interlayer spacing of graphene oxide [12]. The XRD pattern of graphene oxide/TiO_2 nanocomposite has been mainly composed of the anatase and rutile TiO_2 phases (Fig. 5b). The major peaks at $2\theta=25.34^o$, 37.90^o, 48.15^o, 54.07^o, 55.17^o and 62.78^o belong to the diffractions of the (101), (004), (200), (105), (211) and (002) crystal planes of the anatase phase in TiO_2 (Joint Committee on Powder Diffraction Standards card No.21-1272) [12]. On the other hand, the major peaks shown at $2\theta=27.53^o$ and 36.16^o may be attributed to the (110) and (101) crystal planes of rutile phase in TiO_2 (Joint Committee on Powder Diffraction Standards card No. 21-1276) [12]. Because of the stacking disorder caused by the intercalation of TiO_2 particles into stacked graphene oxide layers, the characteristic diffraction peak of graphene oxide has been absent in graphene oxide/TiO_2 nanocomposite pattern [12].

Estimation of CO_2 selectivity over N_2, prediction, and validation of CO_2 adsorption capacity

The Toth isotherm parameters of the pure components used to calculate the reduced spreading pressure and estimate CO_2 selectivity over N_2 in the CO_2:N_2 binary gas mixtures are illustrated in Table. 1. The parameter K_T defined as the adsorption affinity has been assessed to be 0.308×10^{-2} 1/kPa and 0.156×10^{-2} 1/kPa for CO_2 and N_2 molecules, respectively. The Toth parameter t which represents the system heterogeneity and the interaction and mobility of the gas molecules adsorbed (adsorption affinity) on the adsorbent has been assessed to be 0.302 and 1.683 for pure CO_2 and pure N_2 adsorption isotherms, respectively. The value of this parameter (if $t<1$) indicates that the system, including CO_2 molecules and synthesized mesoporous graphene oxide/TiO_2 nanocomposite, is heterogeneous. On the other hand, the t value greater than unity for N_2 adsorption indicates that the adsorptive potential of N_2 molecules on synthesized graphene oxide/TiO_2 nanocomposite is weaker than the lateral interactions between the N_2 adsorbed molecules [12]. The greater affinity for CO_2 molecules over N_2 molecules on the synthesized graphene oxide/TiO_2 nanocomposite concluded by the difference between physical properties of CO_2 molecules and N_2 molecules is led to the higher selectivity of CO_2 molecules versus N_2 molecules on the synthesized graphene oxide/TiO_2 nanocomposite. The most important of these properties

Table 1: Toth isotherm parameters for pure CO_2 ، pure N_2 adsorption at 298 K.

Adsorbate	q_s (mmol/g)	K_T (1/kPa)	t	r^2	Reference
Pure CO_2	35.806	0.308×10^{-2}	0.302	0.9995	This study
Pure N_2	1.433	0.156×10^{-2}	1.683	0.9999	This study

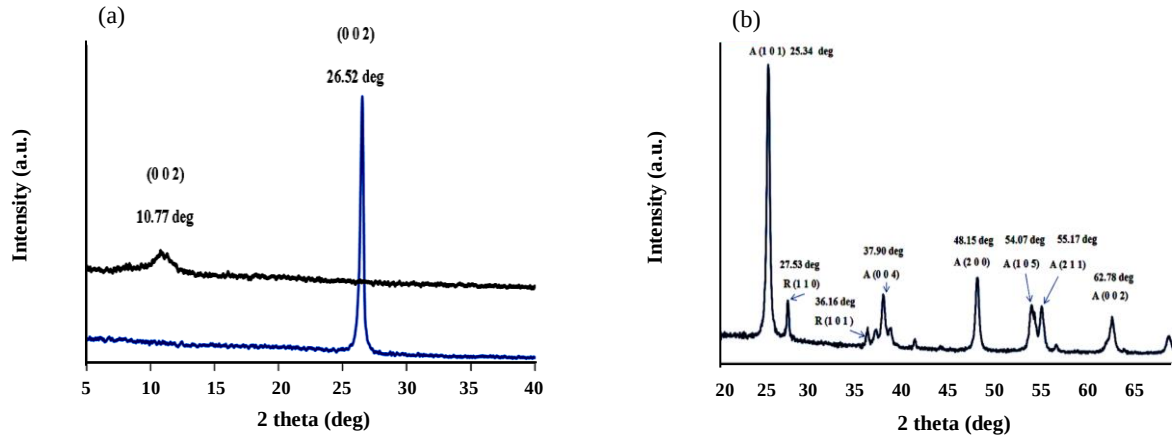

Fig. 5: XRD patterns of graphite and graphene oxide (a) and graphene oxide/TiO_2 nanocomposite (b).

are polarizability and quadrupole moment. The ratios of polarizability and quadrupole moment of CO_2 molecule over N_2 molecule are 1.672 and 2.851, respectively [12]. In addition, CO_2 molecules are more condensable than N_2 molecules because CO_2 has a higher critical temperature (304.1 K) in comparison with that of N_2 (126.2 K) (*Li et al.*, 2015). Fig. 6a, 6b, and 6c show the curve of the reduced spreading pressure versus the molar fraction of CO_2 in the synthesized graphene oxide/TiO_2 nanocomposite at different total pressures and 298 K for different CO_2 concentrations. As shown in this figure, the equilibrium molar fraction (iso-spreading pressure condition) at 1 bar has been predicted to be 0.780, 0.700 and 0.570 for the binary mixtures, including CO_2:N_2=15:85, 10:95 and 5:95, respectively. In this study, these curves have been calculated for 14 total pressures to predict the equilibrium molar fraction of CO_2 with respect to the different CO_2 concentrations in the adsorbed mixture. Subsequently, the selectivity of CO_2 molecules over N_2 molecules on the synthesized graphene oxide/TiO_2 nanocomposite has been estimated. The values of selectivity (Fig.6d) decrease when the pressure increases. This behavior is explained by the fact that, the CO_2 molecules (as the stronger adsorbate component) prefer the high energy sites in comparison with the N_2 molecules (as the weaker adsorbate component) which prefer the weaker adsorption sites. Therefore, the greater amount of CO_2 molecules is adsorbed at lower pressures [33]. Furthermore, when the pressure increases and the high energy sites are filled, the CO_2 molecules begin to compete with the N_2 molecules for the weaker sites which have the lower local values of selectivity [33]. For the case of y_{CO2}= 0.15, which is a typical composition of coal-fired steam power plant [13,14], the selectivity is in the range of 20.09-60.187. For the case of y_{CO2}=0.1, which is the typical composition of oil-fired steam power plant [13,14], the selectivity is in the range of 21-44.886. For the case of y_{CO2}=0.05, which is the typical composition of gas turbine and combined cycle power plant [13, 14], the selectivity is in the range of 25.185-49.476. For these conditions, the selectivity of CO_2 molecules over N_2 molecules (at 1 bar and around 298 K) on the synthesized graphene oxide/TiO_2 nanocomposite in these binary mixture systems is higher than the parameter on other adsorbents, including MOF-508b (selectivity=6, CO_2:N_2=50:50), zeolite NaY (selectivity=14.5, CO_2:N_2=50:50), molecular sieve 5A (selectivity=4.7, CO_2:N_2=50:50), activated carbon (selectivity=6.1, CO_2:N_2=50:50), MIL-53 (Al) (selectivity=10.1, CO_2:N_2=50:50), zeolite beta

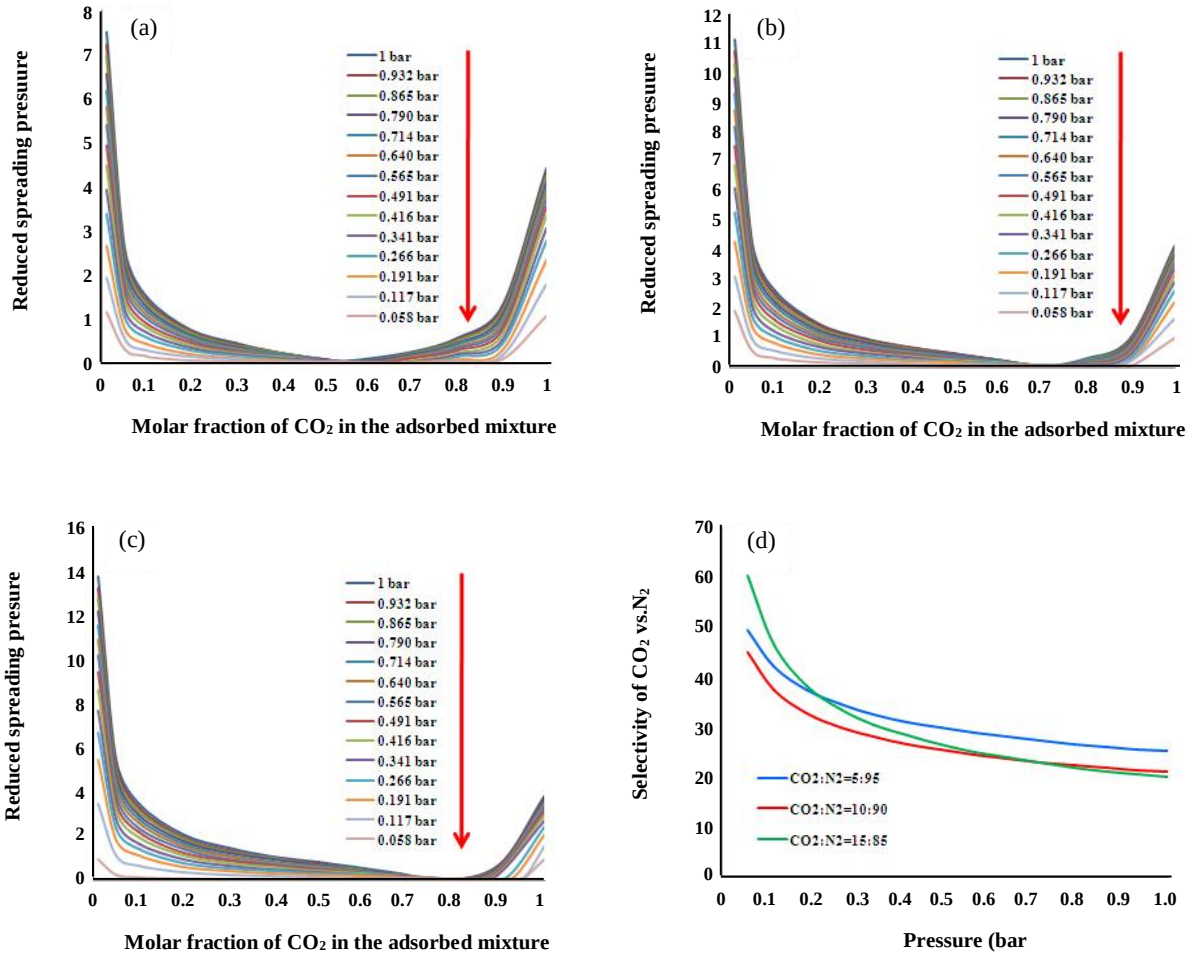

Fig. 6: Reduced spreading pressure as a function of the molar fraction of adsorbed CO_2 for CO_2:N_2=5:95 (a), 10:90 (b), 15:85 (c) and selectivity of CO_2 over N_2 on graphene oxide/TiO_2 nanocomposite (d).

(selectivity=12.5, CO_2:N_2=50:50), Na-SAPO-34 (selectivity=11.66, CO_2:N_2=50:50), SAPO-43 (selectivity=15.28, CO_2:N_2=50:50) NaETS-4 (selectivity=18.35, CO_2:N_2=50:50) [34-38].

Fig.7a illustrates CO_2 adsorption isotherms calculated by the ideal adsorbed solution theory solved with the direct search minimisation. According to this figure, the maximum CO_2 adsorption capacity for CO_2/N_2 binary gas mixture, including CO_2:N_2=15:85, 10:90 and 5:95 were predicted to be 0.954 mmol/g, 0.771 mmol/g and 0.553 mmol/g at 298 K, respectively. To evaluate the reliability of CO_2 adsorption prediction by this method, the breakthrough experiments with the aforementioned simulated flue gas composition were conducted at 1 bar and 298 K (Fig. 7b). According to Fig. 7b, the stoichiometric time for CO_2 =15%, 10% and 5% was calculated to be 138.1 sec, 144.5 sec, and 169.5 sec, respectively. The CO_2 adsorption capacity for CO_2 =15%, 10% and 5%, was measured to be 0.987±0.052 mmol/g, 0.837±0.045 mmol/g and 0.508±0.032 mmol/g respectively. The relative errors between the measured and predicted data were calculated to be 3.343%, 7.885%, and 8.858% respectively. As a result, the ideal adsorbed solution theory solved with the direct search inimisation predicted the experimental data with an appropriate degree of accuracy and uncertainty with respect to different CO_2 concentrations.

These measured CO_2 adsorption capacities are higher than (or comparable with) those reported by Chowdhury et al.[39,40] for other adsorbents, such as acid treated bentonitic clay (0.58 mmol/g for pure CO_2), Cu-MOF (0.65 mmol/g for pure CO_2), γ-Alumina (0.68 mmol/g

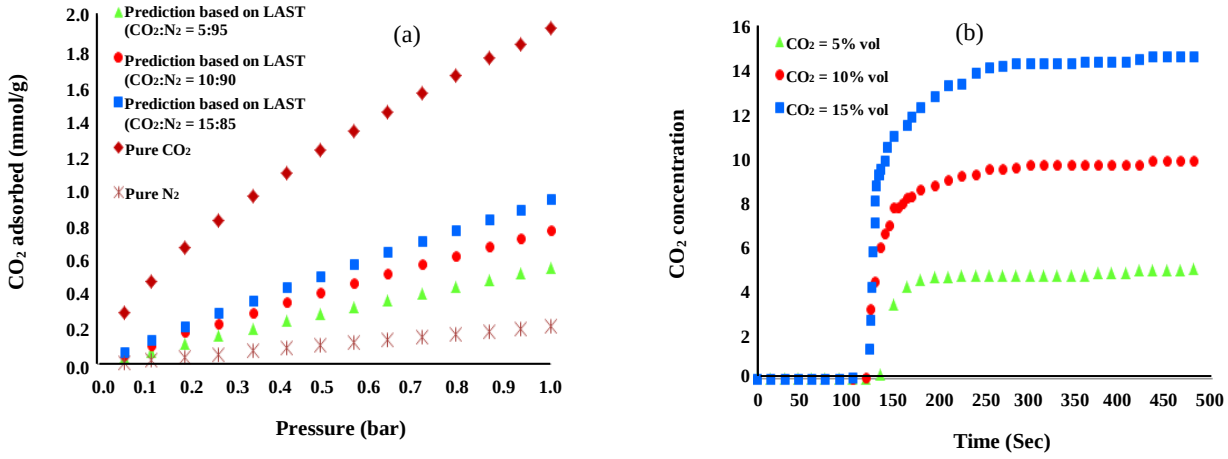

Fig. 7: CO_2 adsorption prediction based on IAST solved with the direct search minimisation (a) and breakthrough experiments with respect to different CO_2 concentrations (b).

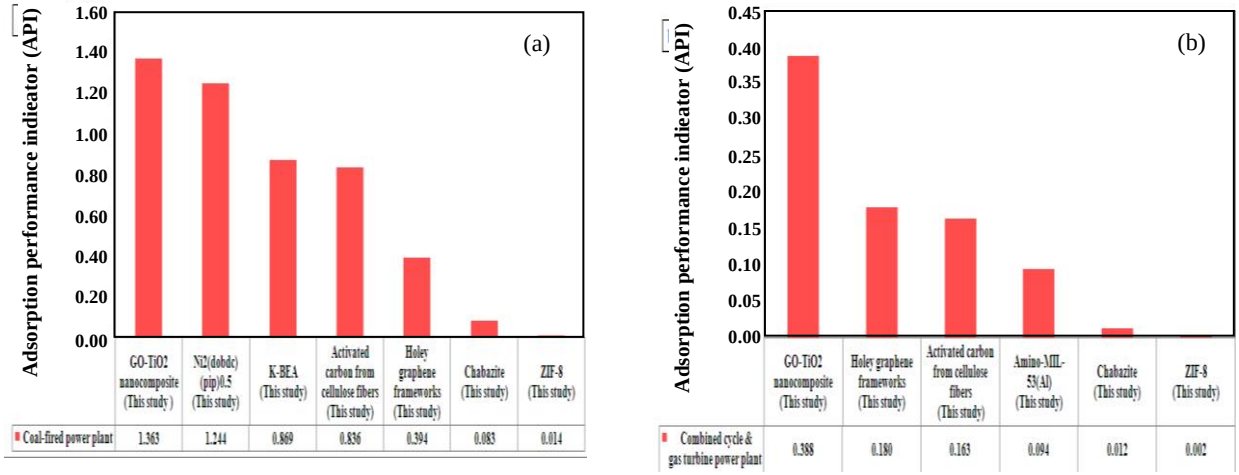

Fig. 8: Adsorption performance indicator values for coal-fired power plant CO_2 capture (a), combined cycle & gas turbine power plant CO_2 capture (b).

for pure CO_2), ZIF-8 (0.11 mmol/g for coal-fired power plant and 0.07 mmol/g for gas turbine and combined cycle power plant), amino-MIL-53(Al) (0.92 mmol/g for coal-fired power plant and 0.22 mmol/g for gas turbine and combined cycle power plant), Chabazite (0.37 mmol/g for coal-fired power plant and 0.13 mmol/g for gas turbine and combined cycle power plant).

Screening thermal power plant CO_2 capture using the adsorption performance indicator

According to the calculation performed in this study, the order of the Adsorption Performance Indicator (API) for CO_2 capture on the synthesized graphene oxide/TiO_2 nanocomposite is a coal-fired power plant (1.363) > oil-fired power plant (0.949)> combined cycle & gas turbine power plant (0.388). This indicator for coal-fired power plant (Fig. 8a) and combined cycle & gas turbine power plant (Fig. 8b) has the highest value in comparison with other adsorbents, including $Ni_2(dobdc)\ (pip)_{0.5}$, K-BEA, activated carbon from cellulose fibers, holey graphene frameworks, Chabazite, ZIF-8 and Amino-MIL-53(Al). As can be seen in Tables 2 and 3, the sequence order of working capacity, the isosteric heat of adsorption of CO_2 and the selectivity of CO_2 over N_2 on these adsorbents are not matched with the order of the adsorption performance indicator values. This observation indicates

Table 2: Parameters related to CO_2 capture for calculation adsorption performance indicator in a coal-fired power plant.

Adsorbents	Selectivity of CO_2 over N_2 at 1 bar	Heat of adsorption (kJ/mol)	Working capacity (mmol/g)	Reference
GO-TiO2	20.090	13.647 [12]	0.987	This study
Ni_2(dobdc) $(pip)_{0.5}$	33	46.200	1.340	[39,41]
K-BEA	26	38.717	1.160	[39,42]
Activated carbon from cellulose fibers	17	27.100	1.190	[39,43]
Holey graphene frameworks	70	49.137	0.530	[39,40]
Chabazite	16	24.856	0.370	[39,44]
ZIF-8	8	5.951	0.110	[39,45]

Table 3: Parameters related to CO2 capture for calculation adsorption performance indicator in gas turbine and combined cycle power plant.

Adsorbents	Selectivity of CO_2 over N_2 at 1 bar	Heat of adsorption (kJ/mol)	Working capacity (mmol/g)	Reference
GO-TiO_2	25.186	16.095 [12]	0.508	This study
Holey graphene frameworks	111	44.572	0.270	[39,40]
Activated carbon from cellulose fibers	23	37.8	0.53	[39,43]
Amino-MIL-53(Al)	23	25.476	0.33	[39,46]
Chabazite	18	24.418	0.130	[39,44]
ZIF-8	9	5.844	0.040	[39,45]

the importance of the API parameter for screening the adsorbents for thermal power plant CO_2 capture in the PSA process.

CONCLUSIONS

The binary CO_2/N_2 selectivity of synthesized mesoporous graphene oxide/TiO_2 nanocomposite using the ideal adsorbed solution theory solved with the direct search minimisation and CO_2 adsorption uptake in the gaseous mixtures of CO_2/N_2 (with respect to CO_2 concentrations in the flue gas of thermal power plants) based on the breakthrough experiment as well as the reported heat of CO_2 adsorption was used in this study to calculate the adsorption performance indicator. The order of the adsorption performance indicator for thermal power plant CO_2 capture on the synthesized mesoporous graphene oxide/TiO_2 nanocomposite is higher than that of other CO_2 adsorbents such as Ni_2(dobdc) $(pip)_{0.5}$, K-BEA, activated carbon from cellulose fibers, holey graphene frameworks, Chabazite, ZIF-8 and Amino-MIL-53(Al). This finding indicates that the aforementioned adsorbent has the appropriate performance in comparison with the common and novel adsorbents for the separation of CO_2 from a CO_2/N_2 mixture similar to the flue gas composition of thermal power plants in the PSA units. The order of the Adsorption Performance Indicator (API) for CO_2 capture on the synthesized graphene oxide/TiO_2 nanocomposite indicates that the coal-fired power plant in comparison with other thermal power plant type (including oil-fired and gas turbine & combined cycle power plants) is the preferred type for the CO_2 separation by the mentioned adsorbent.

Acknowledgments

The authors gratefully acknowledge the financial support of this work (grant no. 94810001) from the Iran National Science Foundation (INSF).

Received : Dec. 6, 2017 ; Accepted : May 21, 2018

REFERENCES

[1] Leung D.Y., Caramanna G., Maroto-Valer, M.M., An Overview of Current status of Carbon Dioxide Capture and Storage Technologies, *Renewable and Sustainable Energy Reviews*, **39**: 426-443(2014).

[2] Balasubramanian R., Chowdhury S., Recent Advances and Progresses in the Development of Graphene-Based Adsorbents for CO_2 Capture, Journal *of Materials Chemistry A*, **3**(44): 21968-21989 (2015).

[3] Sreenivasulu B., Gayatri D.V., Sreedhar I., Raghavan K.V., A Journey into the Process and Engineering Aspects of Carbon Capture Technologies, *Renewable and Sustainable Energy Reviews*, **41**:1324-1350 (2015).

[4] Budzianowski W.M., Single Solvents, Solvent Blends, and Advanced Solvent Systems in CO_2 Capture by Absorption: A Review, *International Journal of Global Warming*, **7**(2): 184-225 (2015).

[5] Banerjee A., Panda S., Sidhantha M., Chakrabarti S., Chaudhuri B., Bhattacharjee S., Utilisation of Eggshell Membrane as an Adsorbent for Carbon Dioxide, *International Journal of Global Warming*, **2**(3): 252-261 (2010).

[6] Wang J., Huang L., Yang R., Zhang Z., Wu J., Gao Y., Wang Q., O'Hare D., Zhong Z., Recent Advances in Solid Sorbents for CO_2 Capture and New Development Trends, *Energy & Environmental Science*, **7**(11): 3478-3518 (2014).

[7] Zhou D., Liu Q., Cheng Q., Zhao Y., Cui Y., Wang T., Han B., Graphene-Manganese Oxide Hybrid Porous Material and its Application in Carbon Dioxide Adsorption, *Chinese Science Bulletin*, **57**(23): 3059-3064 (2012).

[8] Yang S., Zhan L., Xu X., Wang Y., Ling L., Feng X., Graphene-Based Porous Silica Sheets Impregnated with Polyethyleneimine for Superior CO_2 Capture, *Advanced Materials*, **25**(15): 2130-2134 (2013).

[9] Mishra A.K., Ramaprabhu S., Enhanced CO_2 Capture in Fe_3O_4-Graphene Nanocomposite by Physicochemical Adsorption, *Journal of Applied Physics*, **116**(6): 064306 (2014).

[10] Cao Y., Zhao Y., Lv Z., Song F., Zhong Q., Preparation and Enhanced CO_2 Adsorption Capacity of UiO-66/Graphene Oxide Composites, *Journal of Industrial and Engineering Chemistry*, **27**:102-107 (2015).

[11] Wang J., Mei X., Huang L., Zheng Q., Qiao Y., Zang K., Mao S., Yang R., Zhang Z., Gao Y., Guo Z., Synthesis of Layered Double Hydroxides/Graphene Oxide Nanocomposite as a Novel High-Temperature CO_2 adsorbent, *Journal of Energy Chemistry*, 24(2):127-137 (2015).

[12] Chowdhury S., Parshetti G.K., Balasubramanian R., Post-Combustion CO_2 Capture Using Mesoporous TiO_2/Graphene Oxide Nanocomposites, *Chemical Engineering Journal*, **263**: 374-384 (2015).

[13] Goel M., Johri V., "Carbon Capture, Storage and, Utilization: A Possible Climate Change Solution for Energy Industry", India's Climate Change Research Institute, New Delhi, India (2014).

[14] Samanta A., Zhao A., Shimizu G.K., Sarkar P., Gupta R., Post-Combustion CO_2 Capture Using Solid Sorbents: A Review, *Industrial & Engineering Chemistry Research*, **51**(4):1438-1463 (2011).

[15] Walton, K.S., Sholl D.S., Predicting Multicomponent Adsorption: 50 Years of the Ideal Adsorbed Solution Theory, *AIChE Journal*, **61**(9): 2757-2762 (2015).

[16] Belmabkhout Y., Serna-Guerrero R., Sayari A., Adsorption of CO_2 from Dry Gases on MCM-41 Silica at Ambient Temperature and High Pressure. 1: Pure CO_2 Adsorption, *Chemical Engineering Science*, **64**(17): 3721-3728 (2009).

[17] Dickey A.N., Yazaydın A.Ö., Willis R.R., Snurr R.Q., Screening CO_2/N_2 Selectivity in Metal-Organic Frameworks Using Monte Carlo Simulations and Ideal Adsorbed Solution Theory, *The Canadian Journal of Chemical Engineering*, **90**(4): 825-832 (2012).

[18] Karra J.R., Grabicka B.E., Huang Y.G., Walton K.S., Adsorption Study of CO_2, CH_4, N_2, and H_2O on an Interwoven Copper Carboxylate Metal–Organic Framework (MOF-14), *Journal of Colloid and Interface Science*, **392**: 331-336 (2013).

[19] Furmaniak S., Koter S., Terzyk A.P., Gauden P.A., Kowalczyk P., Rychlicki G., New Insights into the Ideal Adsorbed Solution Theory, *Physical Chemistry Chemical Physics*, **17**(11): 7232-7247 (2015).

[20] Pham T.H., Lee B.K., Kim J., Lee C.H., Enhancement of CO_2 Capture by Using Synthesized Nano-Zeolite, *Journal of the Taiwan Institute of Chemical Engineers*, **64**:220-226(2016).

[21] Álvarez-Gutiérrez N., Gil M.V., Rubiera F., Pevida C., Adsorption Performance Indicators for the CO_2/CH_4 Separation: Application to Biomass-Based Activated Carbons', *Fuel Processing Technology*, 142:361-369 (2016).

[22] Wiersum A.D., Chang J.S., Serre C., Llewellyn P.L., An Adsorbent Performance Indicator as a First Step Evaluation of Novel Sorbents for Gas Separations: Application to Metal–Organic Frameworks, *Langmuir*, **29**(10): 3301-3309 (2013).

[23] Monazam E.R., Spenik J., Shadle L.J., Fluid Bed Adsorption of Carbon Dioxide on Immobilized Polyethylenimine (PEI): Kinetic Analysis and Breakthrough Behavior, *Chemical Engineering Journal*, **223**: 795-805 (2013).

[24] Shafeeyan M.S., Daud W.M.A.W., Shamiri A., Aghamohammadi N., Modeling of Carbon Dioxide Adsorption onto Ammonia-Modified Activated Carbon: Kinetic Analysis and Breakthrough Behavior, *Energy & Fuels*, **29**:10: 6565-6577 (2015).

[25] Serna-Guerrero R., Sayari A., Modeling Adsorption of CO_2 on Amine-Functionalized Mesoporous Silica. 2: Kinetics and Breakthrough Curves, *Chemical Engineering Journal*, **161**(1): 182-190 (2010).

[26] Bell S., "A Beginner's Guide to Uncertainty of Measurement", National Physical Laboratory, Teddington, Middlesex, The United Kingdom (2010).

[27] Santori G., Luberti M., Ahn H., Ideal Adsorbed Solution Theory Solved with Direct Search Minimisation, *Computers & Chemical Engineering*, **71**: 235-240 (2014).

[28] Stengl V., Popelková D., Vláčil P., TiO_2–Graphene Nanocomposite as High Performace Photocatalysts, *The Journal of Physical Chemistry C*, **115**(51): 25209-25218 (2011).

[29] Zhang Y., Zhou Z., Chen T., Wang H., Lu W., Graphene TiO_2 Nanocomposites with High Photocatalytic Activity for the Degradation of Sodium Pentachlorophenol, *Journal of Environmental Sciences*, **26**(10): 2114-2122 (2014).

[30] Wu F.C., Wu P.H., Tseng R.L., Juang R.S., Description of Gas Adsorption Isotherms on Activated Carbons with Heterogeneous Micropores Using the Dubinin–Astakhov Equation, *Journal of the Taiwan Institute of Chemical Engineers*, **45**(4): 1757-1763 (2014).

[31] Thommes M., Kaneko K., Neimark A.V., Olivier J.P., Rodriguez-Reinoso, F., Rouquerol, J. and Sing, K.S., Physisorption of Gases, with Special Reference to the Evaluation of Surface Area and Pore Size Distribution (IUPAC Technical Report), *Pure and Applied Chemistry*, **87**(9-10):1051-1069 (2015).

[32] Li W., Jiang X., Yang H., Liu Q., Solvothermal Synthesis and Enhanced CO_2 Adsorption Ability of Mesoporous Graphene Oxide-ZnO Nanocomposite, *Applied Surface Science*, **356**: 812-816 (2015).

[33] Rios R.B., Stragliotto F.M., Peixoto H.R., Torres A.E.B., Bastos-Neto M., Azevedo D.C.S., Cavalcante Jr C.L., Studies on the Adsorption Behavior of CO_2-CH_4 Mixtures Using Activated Carbon, *Brazilian Journal of Chemical Engineering*, **30**(4): 939-951(2013).

[34] Dangi G.P., Munusamy K., Somani R.S., Bajaj H.C., Adsorption Selectivity of CO_2 over N_2 by Cation Exchanged Zeolite L: Experimental and Simulation Studies, *Indian Journal of Chemistry-Part A Inorganic Physical Theoretical and Analytical*, **51**(9): 1238 (2012).

[35] Rallapalli P., Prasanth K.P., Patil D., Somani R.S., Jasra R.V., Bajaj H.C., Sorption studies of CO_2, CH_4, N_2, CO, O_2 and Ar on nanoporous aluminum terephthalate [MIL-53 (Al)]', *Journal of Porous Materials*, 18(2): 205-210 (2011).

[36] Xu X., Zhao X., Sun L., Liu X., Adsorption Separation of Carbon Dioxide, Methane and Nitrogen on Monoethanol Amine Modified β-Zeolite, *Journal of Natural Gas Chemistry*, **18**(2):167-172 (2009).

[37] Shao W., Zhang L., Li L., Lee R.L., Adsorption of CO_2 and N_2 on Synthesized NaY Zeolite at High Temperatures, *Adsorption*, **15**(5-6): 497-505 (2009).

[38] Bae Y.S., Farha O.K., Hupp J.T., Snurr R.Q., Enhancement of CO_2/N_2 Selectivity in a Metal-Organic Framework by Cavity Modification, *Journal of Materials Chemistry*, **19**(15): 2131-2134 (2009).

[39] Chowdhury S., Balasubramanian R., Three-Dimensional Graphene-Based Porous Adsorbents for Postcombustion CO_2 Capture, *Industrial & Engineering Chemistry Research*, **55**(29): 7906–7916 (2016).

[40] Chowdhury S., Balasubramanian R., Holey Graphene Frameworks for Highly Selective Post-Combustion Carbon Capture, *Scientific reports*, **6**: 1-10 (2016).

[41] Das A., Southon P.D., Zhao M., Kepert C.J., Harris A.T., D'Alessandro D.M., Carbon Dioxide Adsorption by Physisorption and Chemisorption Interactions in Piperazine-Grafted Ni_2 (dobdc) (dobdc= 1, 4-dioxido-2, 5-benzenedicarboxylate), *Dalton Transactions*, **41**(38):11739-11744 (2012).

[42] Yang S.T., Kim J., Ahn W.S., CO_2 Adsorption over Ion-Exchanged Zeolite Beta with Alkali and Alkaline Earth Metal Ions, *Microporous and Mesoporous Materials*, **135**(1): 90-94 (2010).

[43] Heo Y.J., Park S.J., A Role of Steam Activation on CO_2 Capture and Separation of Narrow Microporous Carbons Produced from Cellulose Fibers, *Energy*, **91**: 142-150 (2015).

[44] Pham T.D., Xiong R., Sandler S.I., Lobo R.F., Experimental and Computational Studies on the Adsorption of CO_2 and N_2 on Pure Silica Zeolites, *Microporous and Mesoporous Materials*, **185**: 157-166 (2014).

[45] McEwen J., Hayman J.D., Yazaydin A.O., A Comparative Study of CO_2, CH_4 and N_2 Adsorption in ZIF-8, Zeolite-13X and BPL Activated Carbon, *Chemical Physics*, **412**: 72-76 (2013).

[46] Kim J., Kim W.Y., Ahn W.S., Amine-Functionalized MIL-53 (Al) for CO_2/N_2 Separation: Effect of Textural Properties, *Fuel*, **102**: 574-579 (2012).